Fluid Phase Equilibria 520 (2020) 112648

Contents lists available at ScienceDirect

Fluid Phase Equilibria

journal homepage: www.elsevier.com/locate/fluid

Phase stability analysis for tight porous media by minimization of the Helmholtz free energy

Sofiane Haythem Achour , Ryosuke Okuno *

The University of Texas at Austin, USA

ARTICLE INFO

Article history:
Received 19 December 2019
Received in revised form
4 May 2020
Accepted 9 May 2020
Available online 28 May 2020

Keywords:
Phase stability
Capillary pressure
Helmholtz free energy
Equation of state
Shadow-phase region

ABSTRACT

This paper presents a new method of phase stability analysis in the presence of capillary pressure by minimization of the Helmholtz free energy. The thermodynamic consistency of phase stability is rigorously preserved between the Helmholtz and Gibbs free energy.

Case studies demonstrate the main advantages of the new method over the conventional methods using the Gibbs free energy. The effect of capillary pressure on phase stability is inherently considered in the new method using the Helmholtz free energy. The most fundamental reason for various issues associated with using the conventional methods is that the Gibbs free energy in composition space requires a pressure to be specified; i.e., the conventional methods involve two Gibbs free energy surfaces and their relative location changes during the iterative solution with capillary pressure.

Case studies further show that there exist indefinite solutions in phase stability analysis with capillary pressure, in which the fluid is unstable, but no two-phase solution exists. Also, it is demonstrated that the shadow-phase region in the presence of capillary pressure can be defined with the Helmholtz free energy, but not with the Gibbs free energy.

© 2020 Elsevier B.V. All rights reserved.

1. Introduction

Phase equilibrium calculation using an equation of state (EOS) is an essential part of various engineering calculations. Table 1 summarizes the papers published on phase equilibrium calculations in the presence of capillary pressure. The number of publications has increased in response to the recent development of tight reservoirs of oil and gas [1]. As implied in Table 1, it is becoming more important to properly characterize thermodynamic phase behavior in tight porous media and their interplay with transport phenomena. The focus of this paper is on the phase stability problem in the presence of capillary pressure.

The traditional formulation for phase stability analysis uses the Gibbs free energy in composition space at a specified temperature and pressure [2–5]. It is based on the thermodynamic requirement that a phase equilibrium state at a given temperature and pressure is defined by the global minimization of the Gibbs free energy in composition space subject to material balance.

The standard solution method for the isothermal-isobaric phase stability analysis is the stationary point method of Michelsen [3], which locates stationary points of the tangent-place distance (TPD) function and searches for a negative TPD. Any composition identified with a negative TPD value indicates that the fluid tested is an unstable phase. Various methods of phase stability analysis using the Gibbs free energy have been developed and used for engineering purposes, such as stand-alone phase behavior computations and compositional simulation of petroleum reservoirs [6–8]. The fundamental importance of the TPD analysis was recently reconfirmed through the application of TPD to the minimization of the Gibbs free energy for complex multiphase equilibrium calculations [9].

The literature is much scarcer for phase stability analysis in tight porous media. Multiple approaches have been proposed to modeling the effects of capillarity on phase properties in tight porous media [10]. One approach is to modify equations of state to include the effects of pore walls on the bulk fluid [11]. The classical approach models it as a difference between equilibrium phase pressures given by the capillary pressure. The inclusion of capillary pressure can be easily formulated using the TPD function with the phase-specific Gibbs free energy surfaces; however, various implementation problems have been reported in the literature. Only a few major issues are briefly described here. The spinodal

* Corresponding author. Department of Petroleum and Geosystems Engineering, 200 E. Dean Keeton Street, Stop C0300, Austin, TX, 78712, USA.
E-mail address: okuno@utexas.edu (R. Okuno).

https://doi.org/10.1016/j.fluid.2020.112648
0378-3812/© 2020 Elsevier B.V. All rights reserved.

Table 1
Summary of published algorithms in the literature for equilibrium calculations with capillary pressure. "PT" and "TV" represent the thermodynamic specifications used to specify the system.

Authors	Year	Algorithm	P_{cap} model	Specification	Remarks
Brusilovsky [40]	1992	Phase-split calculation	Young-Laplace	PT	Phase-split calculation with capillary pressure.
Shapiro and Stenby [12]	2001	Phase-split calculation	Constant	PT	Study of the spinodal limit at large capillary pressure.
Nojabaei et al. [41]	2013	Phase-split calculation	Young-Laplace	PT	The effect of capillary pressure on phase envelope.
Wang et al. [42]	2013	Phase-split calculation	Saturation-based	PT	Phase-split calculation using saturation-based capillary pressure model.
Sandoval et al. [43]	2016	Phase envelope	Young-Laplace	PT	Efficient way to draw phase envelopes with capillary pressure.
Sherafati and Jessen [15]	2017	Stability analysis	Young-Laplace	PT	Stability analysis for tight porous media.
Yan et al. [35]	2017	Phase-split calculation and stability analysis	Saturation-based	PT	Stability analysis for saturation-based capillary pressure model.
Siripatrachai et al. [44]	2017	Phase-split calculation and stability analysis	Young-Laplace	PT	Negative flash to determine the stability of a mixture.
Rezaveisi et al. [13]	2018	Phase-split calculation	Saturation-based	PT	Study of the spinodal limit in compositional space.
Kou and Sun [23]	2018	Equilibrium calculation	Young-Laplace	TV	Dynamic algorithm for equilibrium calculations.
Neshat et al. [28]	2018	Phase-split calculation	Saturation-based	PT	Demonstration that the conventional root selection is not necessarily correct with large capillary pressure.
Sandoval et al. [45]	2018	Phase-split calculation	Young-Laplace	PT	Phase-split calculation including the compositional effect on adsorption.
Sun and Li [46]	2019	Phase-split calculation	Young-Laplace	PT	Phase-split calculation for three phases with capillary pressure.
Nichita [21]	2019	Stability analysis	Young-Laplace	TV	TV-based stability analysis with capillary pressure.
Lu et al. [47]	2019	Phase-split calculation	Young-Laplace	TV	TV-based flash calculation with capillary pressure.
Sandoval et al. [25]	2019	Phase-split calculation	Saturation-based	PT	Accelerated method for PT flash using molar volume as a variable.
Neshat et al. [15]	2019	Phase-split calculation and stability analysis	Saturation-based	PT	Stability analysis explained in the context of shadow phase region. Demonstration of the issue associated with the non-physical Gibbs free energy region.
Nichita [24]	2019	Phase envelope	Young-Laplace	TV	New method to draw phase envelopes.

boundary of the Gibbs free energy defines the limit of capillary pressure for phase stability analysis [12,13]. This capillary pressure limit makes various implementation problems because the capillary pressure is part of the iterative solution in phase stability analysis using the Gibbs free energy. Although Sherafati and Jessen [14] concluded that the traditional TPD analysis was valid by using the Young-Laplace model with capillary radii of 3−50 nm, Neshat et al. [15] demonstrated another issue that the conventional method using the Gibbs free energy can fail because a non-physical part of the Gibbs free energy (e.g., the vapor side of the Gibbs free energy at a liquid-phase pressure) can cause the TPD to be negative. Hence, the traditional TPD analysis [3] cannot be applied without ad-hoc modifications to the phase stability problem with capillary pressure.

It seems challenging for a computational algorithm to avoid or solve the issues mentioned above in an efficient and robust manner for multicomponent mixtures. Note that negative flash is not equivalent to phase stability analysis as widely known for the traditional phase equilibrium problem with no capillary pressure [16]. The complexity of multicomponent phase behavior with capillary pressure has made it difficult to study the impact of capillary pressure (or tight pores) on fluid flow in tight porous media. Therefore, there is a critical need to develop a fundamental understanding and a robust method of phase stability analysis in the presence of capillary pressure.

The fundamental cause of the issues mentioned above is that the Gibbs free energy requires a pressure to be specified. That is, the conventional phase stability analysis requires two non-linear surfaces in composition space: the Gibbs free energy surface at the reference-phase pressure and another Gibbs free energy surface at the iterative incipient-phase pressure at the specified temperature. Therefore, the Gibbs free energy surface for the incipient phase changes with respect to that of the reference phase during the iteration because the capillary pressure is unknown. This complexity associated with multiple Gibbs free energy surfaces exists also for phase-split calculations with capillary pressure.

One way to address this fundamental issue is to formulate the phase stability analysis with capillary pressure by minimization of the Helmholtz free energy for a given temperature and volume. With no capillary pressure, Nagarajan et al. [17] presented the phase stability analysis using the Helmholtz free energy after Michelsen and Heidemann [18]. Nagarajan et al. [17] showed that the Helmholtz free energy in their variable space was smooth and suitable for gradient-based minimization methods. Mikyška and Firoozabadi [19] explained that the stability analysis using the Helmholtz free energy could not be solved robustly by the traditional successive substitution method. They suggested using Newton's method, which was used by other researchers [20−22].

It is only recently that a few studies were published about the application of the Helmholtz free energy for phase-stability and phase-split calculations in the presence of capillary pressure (Table 1). However, the advantage of using the Helmholtz free energy over the Gibbs free energy is not entirely clear in the literature. For phase stability analysis with capillary pressure, Kou and Sun

[23] presented a derivation of a phase stability criterion including capillary pressure based on the Helmholtz free energy. They used the convex-concave splitting of the Helmholtz free energy to analyze the stability of pure substances and binary mixtures with the Young-Laplace capillary pressure model. They discussed no clear advantage over the conventional methods using the Gibbs free energy. Nichita [21] modified an earlier algorithm for multi-component stability analysis [22] to account for the effect of capillary pressure, by following the derivation by Kou and Sun [23]. However, Nichita [21] presented some inconsistency between the Helmholtz and the Gibbs free energy-based formulations, as will be discussed in this paper. Nichita [21,24] highlighted that using the Helmholtz free energy yields simpler derivatives for volume-explicit capillary pressure functions. This computational advantage was explained also for the volume-based method of phase-split calculations including capillary pressure [25].

In this paper, we present a new formulation and algorithm for phase stability analysis for tight porous media using the Helmholtz free energy. Case studies demonstrate the differences of this paper from recently published papers and the advantages over the conventional methods of phase stability analysis with capillary pressure. Common failures of the conventional methods are explained and solved by the robust method developed in this paper.

This paper is focused on the liquid and vapor phases of hydrocarbon-rich mixtures. The thermodynamic model used is the Peng-Robinson equation of state (EOS) [26] with van der Waals' mixing rules [27]. The capillary pressure is modeled by the Young-Laplace and saturation-based models [28].

2. Formulation and algorithm

This section first presents the formulation for phase stability analysis with a curved interface by using the Helmholtz free energy. Then, the algorithm used for the formulated problem is presented.

2.1. Phase stability analysis with the Helmholtz free energy

The first and second laws of thermodynamics require that the Helmholtz free energy of the system be minimized at an equilibrium state at a specified total molar volume, temperature, and overall composition. With these thermodynamic specifications, a phase is said to be stable if any possible perturbation cannot lower the total Helmholtz free energy of the system. That is, the phase of interest ("reference phase") is stable if

$$dA_{total} = dA_r + dA_\sigma + dA \tag{1}$$

is non-negative for any possible incipient phase. In Equation (1), dA_{total}, dA_r, dA_σ, and dA respectively represent the change in the Helmholtz free energy for the total system, the reference phase, the interface, and the incipient phase. The change in the Helmholtz free energy is

$$dA = -SdT - PdV + \sum_{i=1}^{N_C} \overline{G}_i dN_i \tag{2}$$

for the incipient phase,

$$dA_r = -S_r dT_r - P_r dV_r + \sum_{i=1}^{N_C} \overline{G}_{ir} dN_{ir} \tag{3}$$

for the reference phase, and

$$dA_\sigma = -S_\sigma dT_\sigma - P_\sigma dV_\sigma + \sum_{i=1}^{N_C} \overline{G}_{i\sigma} dN_{i\sigma} + \sigma da \tag{4}$$

for the interface. In the above equations, S is entropy, T is temperature, P is pressure, V is volume, $\overline{G}_i$ is the partial molar Gibbs free energy of component i, σ is the interfacial tension (IFT) between the reference and incipient phases, a is the interfacial area, N_i is the mole number of component i, and N_C is the number of components.

The stability analysis is subject to the material balance, the volume balance, and constant temperature as follows:

$$dN_{ir} + dN_{i\sigma} + dN_i = 0 \tag{5}$$

$$dV_r + dV_\sigma + dV_i = 0 \tag{6}$$

$$dT_r = dT_\sigma = dT = 0. \tag{7}$$

With these constraints, dA_{total} is written as

$$dA_{total} = -(P - P_r)dV - (P_\sigma - P_r)dV_\sigma + \sum_{i=1}^{N_C} \left(\overline{G}_i - \overline{G}_{ir}\right) dN_i + \sum_{i=1}^{N_C} \left(\overline{G}_{i\sigma} - \overline{G}_{ir}\right) dN_{i\sigma} + \sigma da \tag{8}$$

Supposing that the second and fourth terms are negligible in comparison to the other terms on the right-hand side of Equation (8), dA_{total} is approximated as

$$dA_{total} = -(P - P_r)dV + \sum_{i=1}^{N_C} (\overline{G}_i - \overline{G}_{ir}) dN_i + \sigma da. \tag{9}$$

With no loss of generality, dA_{total} is divided by RTdV, which is a positive real number within this stability analysis. Then, the determinant for the phase stability problem is

$$D = dA_{total} \Big/ RTdV = \left[\sum_{i=1}^{N_C} (\overline{G}_i - \overline{G}_{ir}) d_i - (P - P_r) + P_*\right] \Big/ RT, \tag{10}$$

where R is the universal gas constant and $d_i = dN_i/dV$ ($i = 1, 2, \ldots, N_C$) as used by Nagarajan et al. [17]. P_* physically represents $\sigma da/dV$, which depends on the equilibrium phase properties and energy balance with the local interfacial geometries. Note that $d_i = x_i/\underline{V}$ ($i = 1, 2, \ldots, N_C$) and, therefore, $\Sigma d_i = 1/\underline{V}$, where x_i and $\underline{V}$ are the concentration of component i and the molar volume of the incipient phase, respectively. The D function spans the **d** space, and can be considered as the distance between the A/RTV function and the plane that is parallel to the tangent plane to the A/RTV function defined at d_{ir} ($i = 1, 2, \ldots, N_C$) (see Section 3.2 for more details of the function).

The fundamental procedure for the phase stability analysis is to find stationary points of D in **d** space of N_C dimensions, and check the sign of D at the identified stationary points for a given T, $\underline{V}_{total}$, and the overall (or reference-phase) composition x_{ir} ($i = 1,2,\ldots,N_C$). If D is found to be negative at any **d**, the reference phase is determined to be unstable. Note that the location of stationary points is necessary only if the Hessian of the Helmholtz free energy is positive definite at x_{ir}; otherwise, the reference phase is unconditionally unstable.

The stationarity conditions for D in **d** space are derived as

$$F_i = \partial D/\partial d_i = \ln f_i - \ln f_{ir} = 0 \quad (11)$$

for i = 1, 2,…, N_C, for which the Gibbs-Duhem equation is used. In the above equation, f_i is the fugacity of component i. Note that P_* is a scalar value or function to be specified; e.g., the Young-Laplace and saturation-based models relate P_* to properties of the equilibrium phases that satisfy $F_i = 0$ and the associated constraints for all i [29,30]. Hence, the derivative of the P_* term is rigorously zero for the stationarity conditions (see Section 3.1 for more details).

The D function at a stationary point (D_{SP}) is

$$D_{SP} = [-(P - P_r) + P_*] / RT. \quad (12)$$

If $D_{SP} < 0$, $dA_{total} < 0$ at the stationary point identified, noting that $dV > 0$; therefore, the reference phase is determined to be unstable. If $D_{SP} = 0$ at **d** with $x_i \neq x_{ir}$, the incipient and reference phases coexist at an equilibrium phase boundary with $P_* = P - P_r$ as the differential pressure between them. This also reconfirms that a stationary point must satisfy the fugacity equations, Equation (11). In general cases, however, P_* is not directly related to capillary pressure within this research except for phase boundary calculations.

In summary, the phase stability analysis for tight porous media using the Helmholtz free energy is formulated as

find $\mathbf{d}_{sp} \in R^{N_c}$ such that $\mathbf{F} = 0$ and check if $D_{SP} < 0$,
given $\mathbf{F} \in R^{N_c}$ at T, $\underline{V}_{total}$, and $\mathbf{x}_r$ with a specified value or function for P_*.

This analysis is usually repeated using multiple initial guesses because it is generally difficult to ensure that the global minimum of D is located in **d** space using a cubic equation of state. The search for stationary points is a series of local minimization of D in **d** space because the Jacobian matrix of F_i is the Hessian matrix of D.

The formulation above can be also derived by explicitly assuming solid-fluid interfaces in addition to fluid-fluid interfaces.

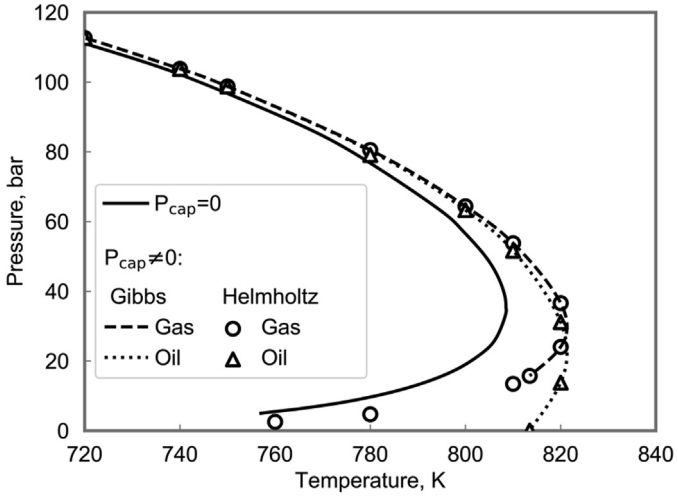

Fig. 1. Dew point curves using the new method and the conventional method for the SJ15 mixture (Table 2). The solid line represents the dew-point curve with no capillary pressure. The dew-point curve for the 10-nm tube is shown by the bold dashed line for the conventional method and by hollow circles for the new method using the Helmholtz free energy. The oil-phase pressures are shown for the phase boundary conditions for the 10-nm tube.

In either way, the formulation given above remains because P_* to be specified by a capillary pressure model should contain such interfacial interactions in tight porous media.

2.2. Algorithm

As in Nichita [22], the independent variables for minimizing D are $\delta_i = 2\sqrt{d_i}$ (i = 1, 2,….,N_C). The thermodynamic model used in this research is the Peng-Robinson EOS [26] with the van der Waals mixing rules [27]. A stationary point of D in δ space is located by local minimization with linear constraints $\sum b_i x_i < \underline{V}$, where b_i is the covolume parameter of component i (i = 1, 2,…., N_C). That is, minimize D(δ) subject to $\mathbf{b}\cdot\mathbf{d} < 1.0$.

A step-wise description of the algorithm for each local minimization is given below. This algorithm is usually repeated for different initial guesses as discussed previously.

Step 1. Calculate the Hessian of D and see if it is positive definite at the reference phase composition, $\mathbf{x_r}$. If it is positive definite, go to Step 2. Otherwise, the reference phase is unstable, and stop.
Step 2. Initialization of **d**

2.1 Initialize the incipient phase **x** and P using the method of the user's choice.
2.2 Solve the equation of state for molar volume of the incipient phase $\underline{V}$.
2.3 Compute the initial **d** and the iteration variables **δ.** Set the iteration index k = 0. $\delta^k = \delta$.

Step 3. Minimization of D using δ

3.1 Compute the gradient of D at δ^k. This gradient is denoted as $\mathbf{g}^k$.
3.2 Compute the Hessian matrix of D at δ^k. This matrix is denoted as $\mathbf{H}^k$.
3.3 Solve for the Newton direction $\Delta\delta^k$ through the modified Cholesky decomposition. $\mathbf{H}^k$ is modified if it is weakly positive definite or non-positive definite.

$$\mathbf{H}^k \Delta\delta^k = -\mathbf{g}^k$$

3.4 Use the line-search technique to optimize the step-size [22] and confirm the feasibility of the iterate: $\mathbf{b}\cdot\mathbf{d} < 1.0$. If unfeasible, reduce the step size λ until δ^{k+1} becomes feasible.

$$\delta^{k+1} = \delta^k + \lambda\Delta\delta^k$$

$$k \leftarrow k + 1$$

3.5 Compute $\mathbf{d}^k$, $\underline{V} = (\sum d_i)^{-1}$, P, and $\mathbf{x}^k = \underline{V}\,\mathbf{d}^k$. Then, calculate the residual $r^k = ||\mathbf{g}^k||_\infty$. If $r^k < \varepsilon_{sp}$, continue to Step 4. Otherwise, go to Step 3.2.

Step 4. Check the proximity of **x** to $\mathbf{x_r}$. If $||\mathbf{x} - \mathbf{x_r}||_\infty > \varepsilon_{ts}$, **x** is considered as a non-trivial stationary point and continue to Step 5. Otherwise, stop.

Table 2
Fluid properties for the SJ15 mixture as given in Ref. [14]. Other binary interaction parameters are all zero. This fluid is used for case studies in section 3.1 and 3.4.

	Composition	T_c	P_c	ω	Parachor	Binary interaction parameters		
	mol fraction	K	bar			N_2	CO_2	C_1
N_2	0.0018	126.2	34.045	0.04	43.85	0		
CO_2	0.0082	304.2	73.866	0.228	82.24	0.017	0	
C_1	0.2292	190.6	46.002	0.008	71.52	0.0311	0.12	0
C_2	0.0721	305.4	48.839	0.098	113.71	0.0515	0.12	0
C_3	0.0737	369.8	42.455	0.152	151.14	0.0852	0.12	0
i-C_4	0.0158	408.1	36.477	0.176	181.78	0.1033	0.12	0
n-C_4	0.0523	425.2	37.997	0.193	191.03	0.08	0.12	0
i-C_5	0.0225	460.4	33.843	0.227	224.14	0.0922	0.12	0
n-C_5	0.036	469.6	33.741	0.251	231.73	0.1	0.12	0
C_6	0.0484	507.4	29.688	0.296	274.03	0.08	0.12	0
PS1	0.196107	565.85	29.708	0.34612	331.01	0.08	0.1	0.028349
PS2	0.113893	683.44	20.103	0.57838	546.37	0.08	0.1	0.044813
PS3	0.066598	798.99	13.324	0.90175	884.73	0.08	0.1	0.062256
PS4	0.041047	899.68	9.697	1.19183	1391.97	0.08	0.1	0.077679
PS5	0.022355	1013.31	7.670	1.39383	2497.41	0.08	0.1	0.0952

Table 3
Critical properties for the equimolar C_1/n-C_{10} mixture use for section 3.2.

Component	T_c	P_c	ω	Binary interaction parameters	
	K	Bar		C_1	n-C_{10}
C_1	190.7	46.0	0.008	0	0
n-C_{10}	617.6	21.1	0.49	0	0

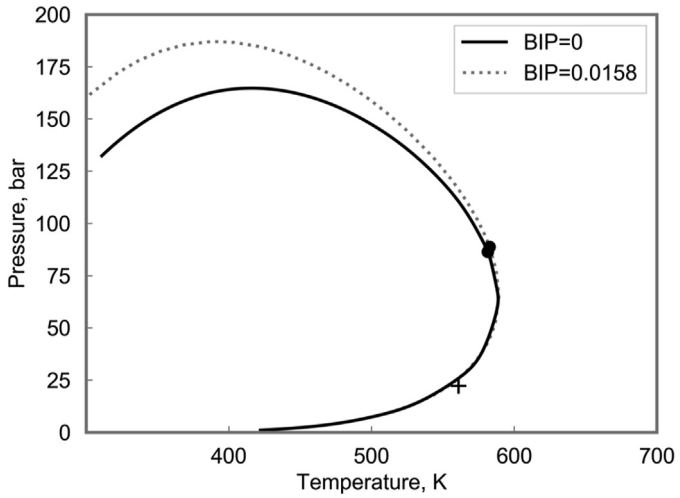

Fig. 2. Phase envelope for the equimolar methane/n-decane mixture (Table 3). The conditions for section 3.2 are marked by the "+" sign, 560.9 K and 22.3 bar. The BIP used are 0 for the solid curve and 0.0158 calculated from Kumar [36] for the dotted curve.

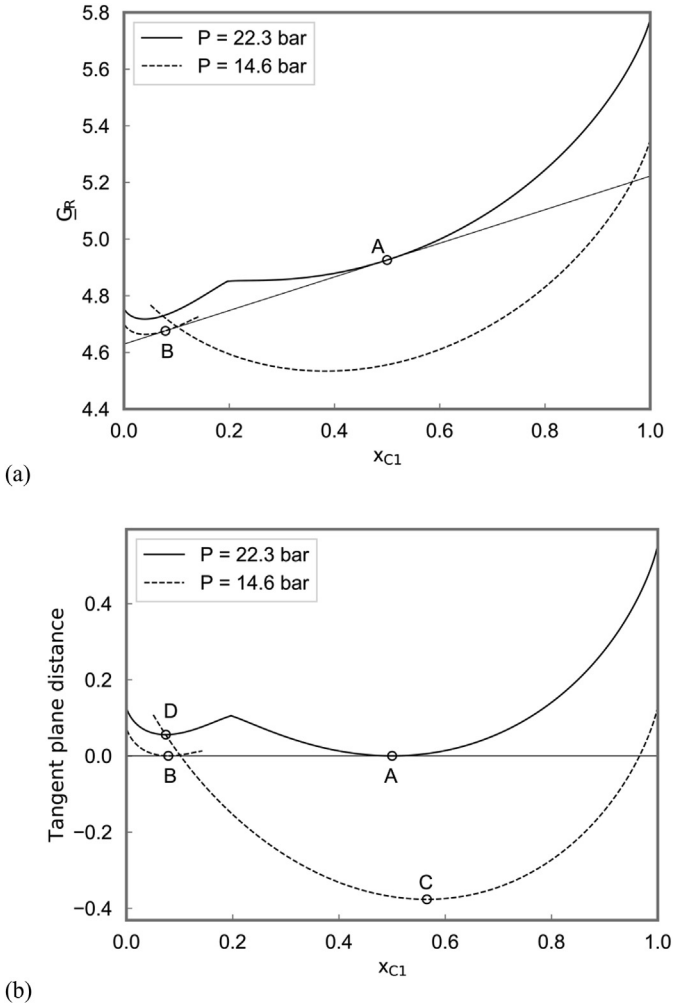

Fig. 3. Reduced Gibbs free energy, $\underline{G}_R$, (a) and tangent-place distance (b) for the C_1/n-C_{10} binary system (Table 3) at 560.9 K for the reference equimolar mixture A at 22.3 bar. Point B is the incipient phase composition at 14.6 bar. Points C and D are additional stationary points at 14.6 bar and 22.3 bar, respectively.

Step 5. Calculate D_{sp} at **x**. If $D_{sp} < 0$, the reference phase $\mathbf{x_r}$ is unstable.

If all tested initial guesses do not find the reference phase to be unstable, it is assumed to be stable. Remarks for some steps are given here. In Step 2.1, a common choice [19,22] is to use Raoult's law along with a certain vapor-pressure correlation (e.g., Wilson's correlation [31]) for either vapor-like or liquid-like phase; however, other initialization methods have been also proposed [17,20,32]. In Step 2.2, if there are two real roots, both roots can be tested as presented by Mikyška and Firoozabadi [19]. In Step 3.5, the EOS is used to explicitly compute P by using $\underline{V}$. Hence, this algorithm does

not involve the potential issue associated with the root selection of a cubic EOS as described in Neshat et al. [28]. Note that P_* does not need to be estimated in Step 3. In Step 5, P_* is specified as a scalar quantity or function. The Young-Laplace and saturation-based models as given in Appendices A, B, and C represent simplified correlations that are often used to estimate equilibrium capillary pressure in porous media for phase behavior calculations [13–15,21,23–25,28] and are used in the case studies in this paper. More elaborate models have also been presented in the literature with the geometrical information of interfaces in a pore network [33]. In this research, ε_{sp} and ε_{ts} are 10^{-9} and 10^{-4}, respectively. Appendix D presents a flow chart of the algorithm.

3. Case studies

The main objective of this section is to demonstrate the main advantages of using the Helmholtz free energy over the conventional method using the Gibbs free energy [15] for phase stability analysis with a curved interface. The thermodynamic model used is the Peng-Robinson EOS [26] with the van der Waals mixing rules [27]. Volume shift is not used within this research as it affects the fugacity equations when equilibrium phases have different pressures [34]. The conventional method compared with the new method here is based on Neshat et al. [15] with slight modifications. A brief summary of Neshat et al.'s method is as follows: Step 1. Set the capillary pressure

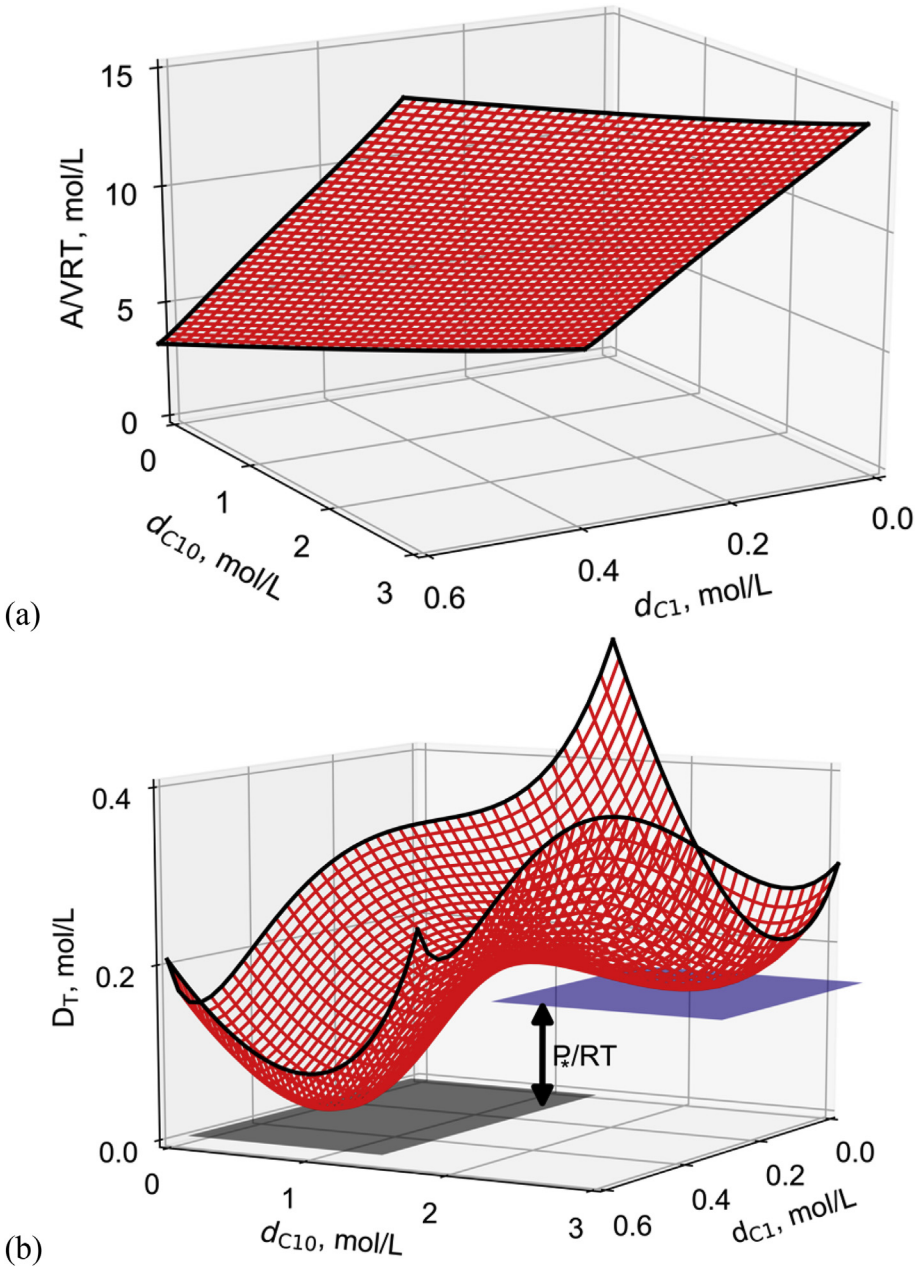

Fig. 4. (a) Helmholtz free energy (A/RTV) in **d** space for the binary system given in Table 3 at 560.9 K and 1.176 L/mol. (b) TPD function, D_T (Equation (15)), for the equimolar mixture of methane and n-decane (Table 3) at 560.9 K and 1.176 L/mol. The purple plane represents the base plane for D (Equation (10)) and the grey plane represents the base plane for D_T (Equation (15)). $D - D_T$ gives P_*/RT.

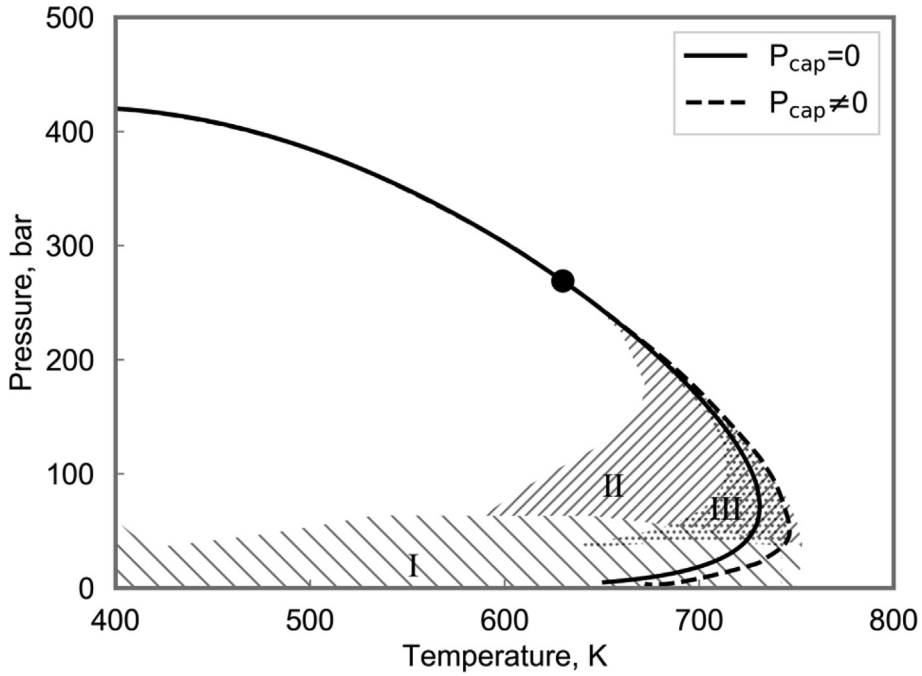

Fig. 5. Phase envelopes for the equimolar mixture of methane and Eagle Ford light oil with and without capillary pressure. Regions I and II represent the conditions for non-convergence with the conventional methods as described in Section 3.3 while Region III shows the conditions for indefinite solutions. Section 3.3 defines the indefinite solution when the overall mixture is unstable, but has no two-phase equilibrium solution.

Table 4
Peng-Robinson EOS fluid model for the equimolar mixture of Eagle Ford light oil and methane [37]. This fluid is used for sections 3.3 and 3.4.

	Composition	Molecular weight	Critical pressure	Critical temperature	Acentric factor	Parachor
	mole fraction	g/mol	bar	K		
N_2	0.000365	28.01	33.9349143	126.2	0.04	41
CO_2	0.006410	44.01	73.8431786	304.222222	0.225	78
C_1	0.656155	16.04	46.3944429	190.7	0.013	77.3
C_2	0.021570	30.07	48.8255536	305.427778	0.097	108.9
C_3	0.020740	44.1	42.5551214	369.888889	0.152	151.9
i-C_4	0.006750	58.12	36.46735	408.111111	0.185	181.5
n-C_4	0.016910	58.12	37.9562071	425.222222	0.201	191.7
i-C_5	0.009025	72.15	33.3269643	460.388889	0.2223	225
n-C_5	0.010705	72.15	33.7419143	469.783333	0.2539	233.9
n-C_6	0.023115	86.18	30.3078929	507.888889	0.3007	271
$C_{7\text{-}10}$	0.081485	112	27.7644286	589.166667	0.3739	311
$C_{11\text{-}14}$	0.060020	175	21.2093214	679.777778	0.526	471
$C_{15\text{-}19}$	0.050220	210	16.6393571	760.222222	0.6979	556.3
C_{20+}	0.036530	250	10.4151071	896.777778	1.0456	836.4

to 0. Use the stability analysis of Michelsen [3] with no capillary pressure. If only the trivial solution is obtained, the mixture is assumed to be stable. Otherwise, go to Step 2. Step 2. Perform a phase-split calculation at a fixed capillary pressure, and then update the capillary pressure using the Young-Laplace or saturation-based model. Step 3. Perform a stability analysis at the given capillary pressure [3,15,35] and return to Step 2. At convergence, the positivity/negativity of the TPD at the stationary points given by Step 3 determines the stability/instability of the mixture tested.

3.1. Case 1

The main objective of Case 1 is to clarify the differences between this paper and other publications on phase stability analysis with capillary pressure [21,23]. Kou and Sun [23] presented their derivation of the phase stability criterion using the Helmholtz free energy in the presence of capillary pressure, which is quite different from that in this paper (Section 2.1).

The important consequence of the differences lies in the P_* term. To obtain the result of Kou and Sun [23], this term must be replaced by γP_{cap}, where $\gamma = 1$ for a gas phase and $\gamma = -1$ for a liquid phase. Then, their stationarity criterion contained the derivative of γP_{cap} with respect to their independent variables, which are the component mole numbers in the incipient phase. Kou and Sun's [23] derivation resulted in the statement of Nichita [24] that $F_i = 0$ is not the stationarity condition of the D function in **d** space.

As described previously, use of P_* as differential pressure between two phases necessitates that $dA_{total} = 0$ in **d** space and, therefore, $F_i = 0$ for $i = 1, 2, \ldots, N_C$. That is, only if the stationarity conditions (i.e., fugacity equations) are satisfied, P_* can be specified

Table 5
Non-zero binary interaction parameters for the fluid shown in Table 4 [37]. This fluid is used for sections 3.3 and 3.4.

	N_2	CO_2	C_1	C_2	C_3	i-C_4	n-C_4	i-C_5	n-C_5
N_2	0								
CO_2	−0.02	0							
C_1	0.036	0.1	0						
C_2	0.05	0.135	0	0					
C_3	0.08	0.135	0	0	0				
i-C_4	0.095	0.13	0	0	0	0			
n-C_4	0.09	0.13	0	0	0	0	0		
i-C_5	0.095	0.125	0	0	0	0	0	0	
n-C_5	0.1	0.125	0	0	0	0	0	0	0
n-C_6	0.1	0.125	0	0	0	0	0	0	0
$C_{7\text{-}10}$	0.151	0.111	0.025	0.02	0.015	0.111	0.005	0.005	0.005
$C_{11\text{-}14}$	0.197	0.097	0.049	0.039	0.029	0.097	0.01	0.01	0.01
$C_{15\text{-}19}$	0.235	0.085	0.068	0.054	0.041	0.085	0.014	0.014	0.014
C_{20+}	0.288	0.07	0.094	0.075	0.056	0.07	0.019	0.019	0.019

Table 6
Capillary pressure parameters used for section 3.3, as given in Neshat et al. [28]. The equation and parameters are defined in Appendix C. The permeability, S_{omin} and S_{gmin}, do not follow Neshat et al. [28]; they were altered to reproduce a similar rock that presents a more challenging phase behavior calculation.

	S_w	ϕ	k μD	b_o	b_g	a_o	a_g	S_{omin}	S_{gmin}
3.88	0	0.07	0.1	0.386	−0.193	1.0	0.06	0.05	0.05

by using a capillary-pressure model, for example, by the Young-Laplace or saturation-based model. Hence, the derivative of the P_* term must be zero for the stationarity conditions of D. This can be also confirmed when the method in this research is applied to a phase boundary, at which $D_{SP} = 0$ at $\mathbf{d}$ with $x_i \neq x_{ir}$ that satisfies Equation (11). In essence, the phase stability problem in this research is to find stationary points of D, and to check for each stationary point to see if the reference phase is stable or unstable assuming the identified stationary point and the reference phase coexist as equilibrium phases (i.e., stationary points satisfy Equation (11)).

The γP_{cap} term remained in the stationarity conditions derived by Kou and Sun [23] and Nichita [21]. In the case of Nichita [21], for example, it is given as

$$\ln f_i - \ln f_{ir} + \partial P_{cap}/\partial d_i = 0 \tag{13}$$

for $i = 1, 2, \ldots, N_C$. Therefore, the component fugacities are not equal between the reference phase and a stationary point found by their methods, as confirmed in this research. This is likely the reason why calculation results were inconsistent between Nichita's [21] method using the Helmholtz free energy and a method using the Gibbs free energy [14]. Nichita [21] showed in Fig. 1 of his paper that the dew point curve by his Helmholtz-free-energy method deviated from the one using the Gibbs free energy for the fluid "SJ15" taken from Sherafati and Jessen [14]. However, the results for a given thermodynamic problem must be identical whether the problem is formulated by minimization of the Helmholtz free energy or the Gibbs free energy.

The new method developed in this research is used to calculate dew point curves for the fluid "SJ15" with no curved interface and with a capillary radius of 10 nm for the Young-Laplace model (Table 2). The IFT and capillary pressure models used are described in Appendices A and B. As in their papers, a Parachor exponent of 4 is used. Unlike in Sherafati and Jessen [14] and Nichita [21], the Peng-Robinson equation of state is used with no volume shift here, but it is used for both approaches using the Gibbs and Helmholtz free energy for a fair comparison.

Fig. 1 showed the calculated dew point curves using the new method and the conventional method using the Gibbs free energy [15]. The capillary tube's surface is assumed to be liquid-wet; therefore, capillary pressure causes the two-phase region to expand in this diagram. The dew-point curve without capillary pressure is given by the solid line. The dew-point curve for the 10-nm tube is shown by the bold dashed line for the conventional method and by hollow circles for the new method using the Helmholtz free energy. The figure also shows the oil-phase pressures for the phase boundary conditions for the 10-nm tube. As expected, the new and conventional methods give the identical results, confirming the consistency between the Helmholtz and Gibbs formulations.

3.2. Case 2

Unlike the conventional methods using the Gibbs free energy, the new method involves only a single Helmholtz free energy surface, which improves the robustness especially for small pores (i.e., high capillary pressure). The conventional methods involve two Gibbs free energy surfaces for phase stability analysis: one fixed energy surface for the reference phase and another iterative energy surface for the incipient phase. Since the capillary pressure has to be part of the iterative solution, the conventional methods tend to fail when they attempt to minimize the total Gibbs free energy using two Gibbs surfaces with a large capillary pressure. This case study presents an example to demonstrate the advantage of using the Helmholtz free energy over the Gibbs free energy.

Table 3 shows the fluid properties for the equimolar mixture of methane and n-decane. The temperature is 560.9 K and the reference pressure is 22.3 bar. Fig. 2 shows the P-T diagram in bold with no capillary pressure for this mixture, in which the condition for this case study is marked. The dotted envelope shows the phase envelope using a binary interaction parameter (BIP) obtained by fitting experimental data [36]. The dew point can be reasonably approximated without using BIP in this case. The capillary pressure used for the stability analysis is 7.7 bar. This mixture results in two phases with the oleic-phase pressure of 14.6 bar at the methane concentration of 7.88% as presented in Fig. 3a. The Gibbs free energy is shown by the solid line for the gaseous phase and by the dashed line for the oleic phase. Points A and B represent the reference and incipient phases, respectively.

The distance between the tangent line and the Gibbs free energy in Fig. 3a gives the tangent-plane distance (TPD) as shown in Fig. 3b. The correct solution of the phase stability problem for the reference fluid (Point A) is given by the incipient phase given by Point B. However, Fig. 3b shows a large segment of negative TPD values with the stationary point C. By observation of the two Gibbs free energy surfaces in the entire composition space, this stationary point C can be easily identified as a non-physical part of the Gibbs free energy for the oleic phase. However, it is challenging for a computational algorithm to robustly and efficiently exclude such non-physical parts of the Gibbs free energy surfaces in composition space for general multicomponent mixtures. The fundamental cause of this issue is that the Gibbs free energy in composition space requires a pressure to be specified. This figure clarifies that the conventional phase-stability analysis using the Gibbs free energy cannot be applied without ad-hoc modifications [15] to the phase-stability problems with capillary pressure even for simple binary mixtures.

Fig. 4a shows the Helmholtz free energy (A/VRT) for hypothetically single-phase mixtures (Table 3)

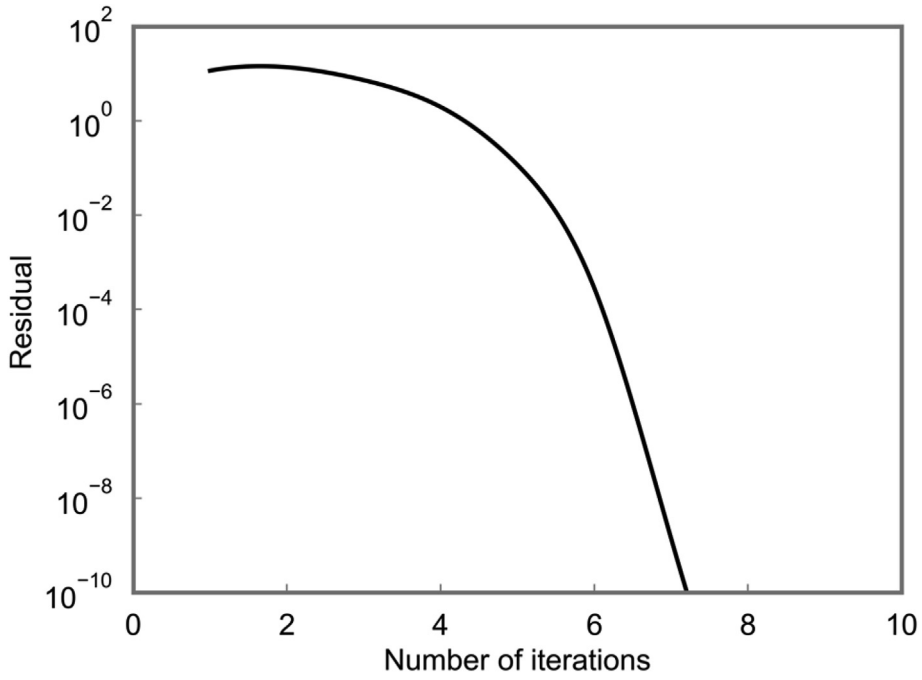

Fig. 6. Convergence behavior of the new algorithm for the mixture given in Tables 4 and 5 at 700 K and the reference phase pressure of 50 bar.

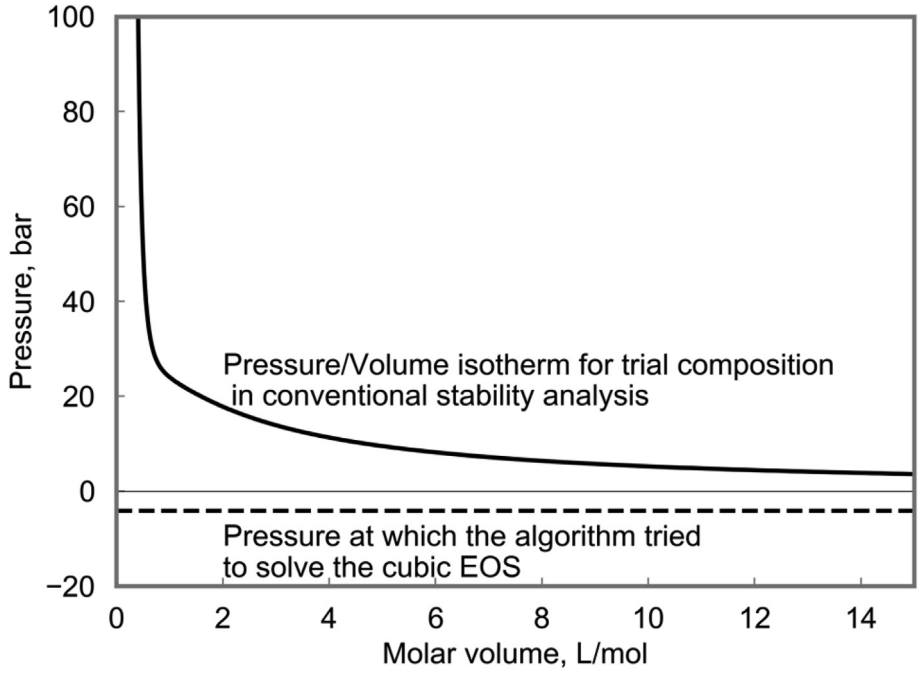

Fig. 7. Pressure-volume curve of the PR EOS when the conventional method failed to solve the EOS for the liquid phase at −4.056 bars during the phase stability analysis for the mixture given in Tables 4 and 5 at 700 K and the reference phase pressure of 50 bar. The new method rapidly converges for this phase stability problem as presented in Fig. 6.

$$A/VRT = d_1 \ln f_1 + d_2 \ln f_2 - P/RT \quad (14)$$

in **d** space at 560.9 K. The vertical axis has a unit of molar density, mol/L. The labels d_{C1} and d_{C10} represent the component molar densities of methane and n-decane, respectively, with the unit of mol/L. The non-linearity of the A/VRT surface is not obvious in Fig. 4a, but it is clearly shown that only one function spans the **d** space. This surface inherently contains the pressure variability given by the fixed temperature and the variable composition $x_i = d_i / \sum_{j=1}^{N_C} d_j$ $(i = 1,\ldots,N_C)$ and molar volume $\underline{V} = 1/\sum_{j=1}^{N_C} d_j$ in the **d** space.

More details of the Helmholtz free energy function in **d** space are described because it is important to have a graphical

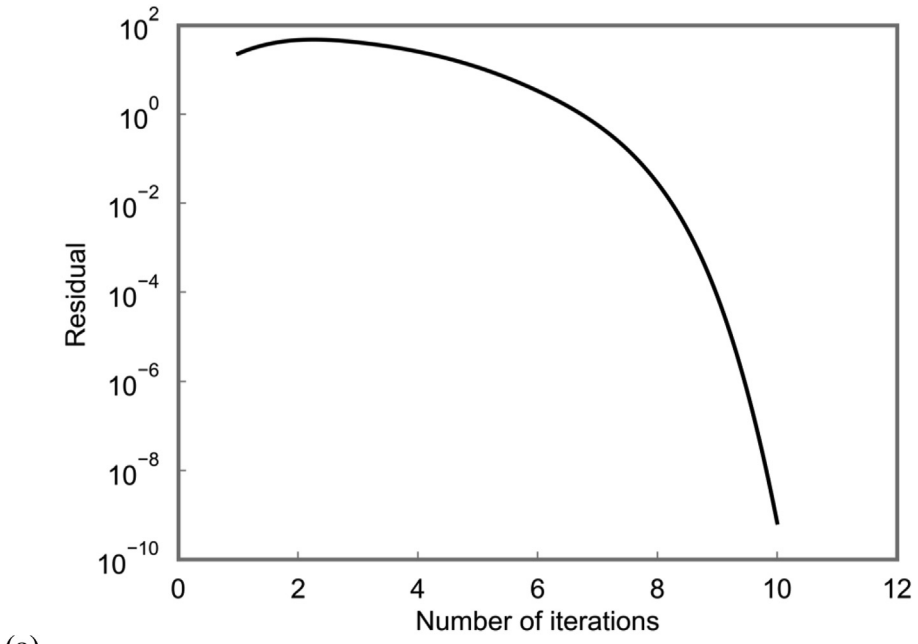

Fig. 8. Convergence behavior for the equimolar mixture of the mixture given in Tables 4 and 5 in region II at 680 K and the reference phase pressure of 170 bar; (a) Rapid convergence behavior of the new algorithm ("residual" is defined in Section 2.2), (b) Non-convergence of the phase-split calculation as part of the conventional method using the Gibbs free energy.

understanding of the function. It is straightforward to derive the expression for the tangent plane onto the A/VRT surface defined at the reference phase by repeating the derivation given in Section 2.1 with $dA_\sigma = 0$. The result corresponds to the determinant for phase stability analysis with no curved interface using the Helmholtz free energy, which is the TPD function as given by

$$D_T = \left[\sum_{i=1}^{N_C}(\overline{G}_i - \overline{G}_{ir})d_i - (P - P_r)\right] \Big/ RT. \tag{15}$$

Fig. 4b shows the D_T function for this case. The reference phase is given by $(d_{C1}, d_{C10}) = (0.284, 0.284)$ mol/L and the incipient phase is $(d_{C1}, d_{C10}) = (0.226, 2.65)$ mol/L. The reference and incipient

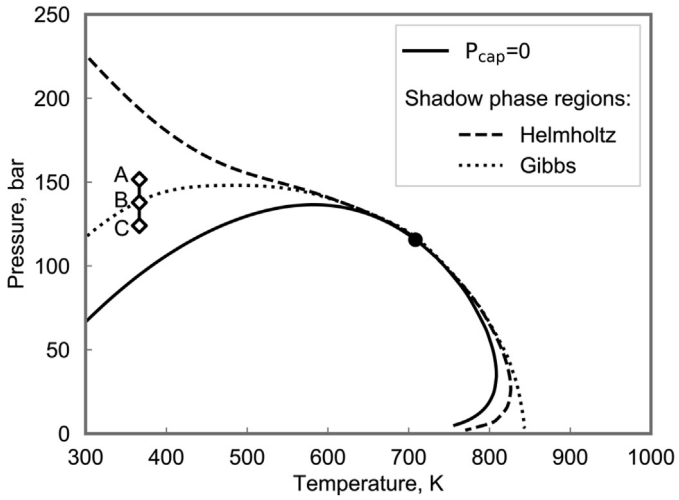

Fig. 9. Helmholtz and Gibbs free energy shadow-phase regions with the SJ15 oil mixture (Table 2). Points A, B, and C at 366.5 K are used for the calculations for Fig. 10.

phases are the ones indicated by points A and B in Fig. 3, respectively. Comparing Equations (10) and (15) indicates that $P_*/RT = D - D_T$ at the incipient phase, which is 0.165 mol/L in this case. The distance between the D_T surface and the purple plane represents the value of D at the stationary point. In this case, the D_T surface is tangent to the purple plane indicating that the reference phase is at equilibrium with the incipient phase.

3.3. Case 3

This section shows that the new method solves two types of inherent difficulties with the conventional methods using the Gibbs free energy. The example used is based on the equimolar mixture of methane and an Eagle Ford oil [37] as shown in Fig. 5 (no volume shift is used). The fluid properties are given in Tables 4 and 5. Phase boundaries are calculated by using the new method with no capillary pressure and with the saturation-based capillary pressure. The capillary pressure model [28] used in this section is described in Appendix C. It uses a Leverett-J scaling function to represent the experimental data [38]. The parameters used for the calculations correspond to the model that was fit to tight rock sample 2 [28] as given in Table 6. The permeability, S_{omin}, and S_{omax} were changed from the original model [28] to increase the capillary pressure as a necessity to illustrate regions of failure of the conventional algorithm using the Gibbs free energy [15] on a PT phase envelope. Regions I and II in Fig. 5 represent the conditions for non-convergence with the conventional methods as described below. Region III shows the conditions of indefinite solutions within the two-phase region.

3.3.1. Region I

In Region I, the conventional method results in non-convergence because of the overshoot of the iterative capillary pressure. This example is presented for the mixture (Tables 4 and 5) at 700 K and the reference phase pressure of 50.0 bar. The new method converges rapidly as shown in Fig. 6 with $D_{SP} = -1.542$ mol/L < 0 indicating that the reference phase is unstable. The conventional method using the Gibbs free energy results in non-convergence when it attempts to solve the EOS for the liquid phase at −4.056 bar. This pressure is lower than the minimum pressure on the pressure-volume isotherm for the liquid composition as shown in Fig. 7. At equilibrium, the liquid pressure is 29.84 bar.

The new method has no such overshoot problems because it does not involve the iterative capillary pressure as shown in Section 2.2. Also, it uses the minimization algorithm with the linear constraints, $\mathbf{b}\cdot\mathbf{d} < 1.0$. It is a standard procedure that keeps the iterate feasible in the algorithm, as used also by Nichita [21,22].

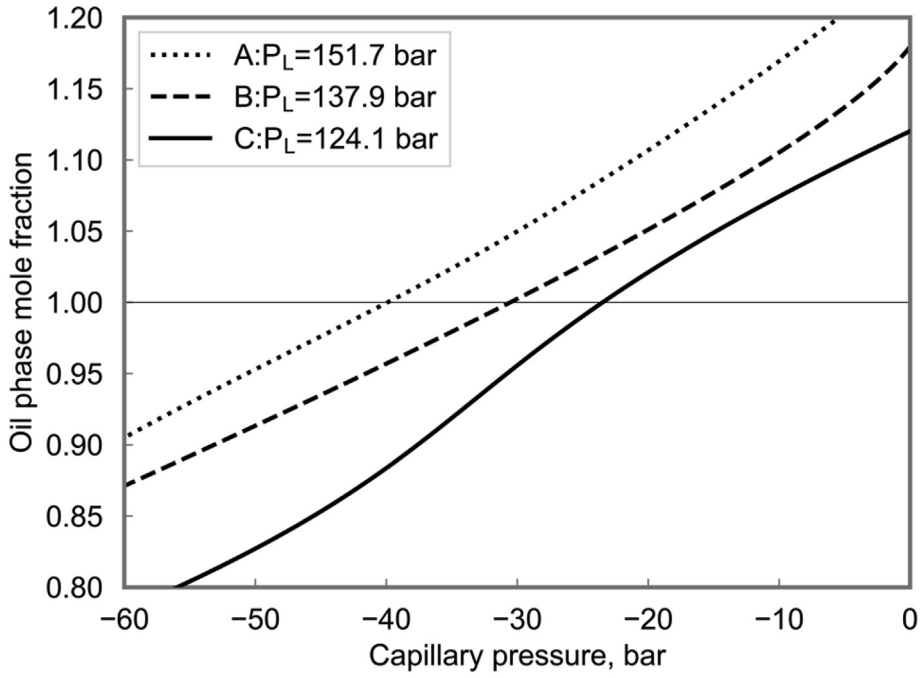

Fig. 10. Oil phase mole fractions calculated at 366.5 K at three different pressures, Points A, B, and C given in Fig. 9. The reference phase pressure is 151.7 bar for Point A, 137.9 bar for Point B, and 124.1 bar for Point C at the temperature of 366.5 K as indicated in Fig. 9.

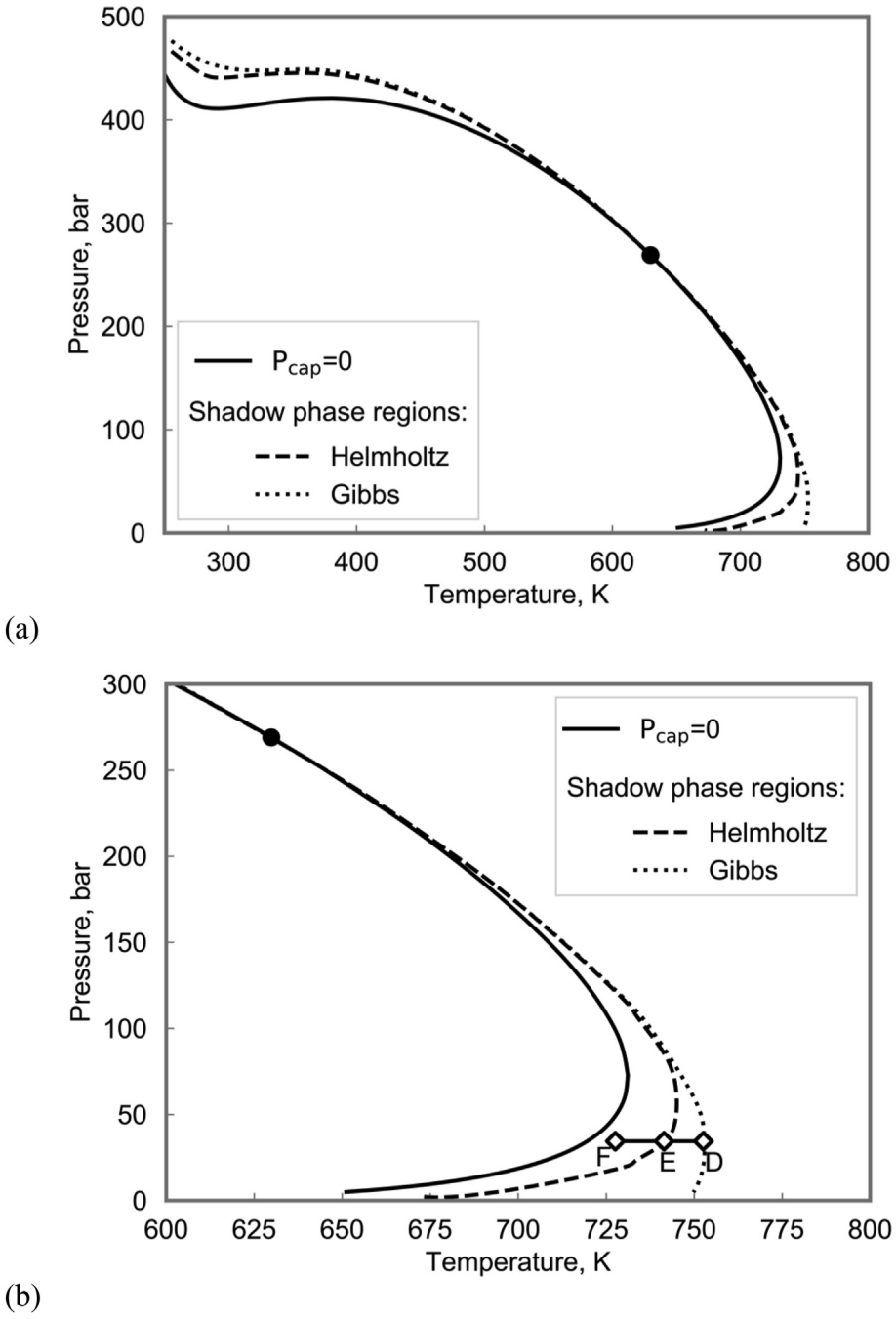

Fig. 11. Helmholtz and Gibbs free energy shadow-phase regions for the equimolar mixture of Eagle ford light oil and methane (Tables 5 and 6); (a) pressure-temperature diagram with the shadow-phase regions; (b) a magnified view for the dew-point side of Fig. 11a. Points D, E, and F at 34.5 bar are used for the calculations for Fig. 12.

3.3.2. Region II

In Region II, the conventional method results in non-convergence because of the absence of any solution to the phase-split calculation as part of phase stability analysis. In previous studies [13,15], the fluid was assumed to be stable when their phase stability analysis methods resulted in this type of non-convergence. However, Fig. 5 clearly shows that Region II exists even within the two-phase envelope. The robustness of the new method enables to demonstrate for the first time that phase stability problems with capillary pressure can yield indefinite solutions as described below.

A specific example is given using the same mixture (Tables 4 and 5) at 680 K and the reference phase pressure of 170 bar. The new method converges rapidly to the solution with $D_{SP} = -0.1046$ mol/L < 0 indicating the instability of the reference phase. Fig. 8a shows the convergence behavior that is quadratic near the solution.

The conventional method using the Gibbs free energy shows non-convergence as shown in Fig. 8b. The main reason for this non-convergence is that the iterative capillary pressure, 20.8 bar, exceeds the capillary pressure, 19.9 bar, at which the iterative liquid-like incipient phase is located at a spinodal point on the Gibbs free energy. With a capillary pressure greater than this limit, no solution exists for two-phase split calculation as explained in Refs. [12,13]. For this specific example, however, the capillary pressure at the equilibrium solution, 16.3 bar, is less than the limiting value of

19.9 bar.

3.3.3. Region III

Region III in Fig. 5 shows the conditions at which the equilibrium capillary pressure is greater than the limiting value inside the two-phase region. This example demonstrates for the first time that indefinite situations can occur even inside a two-phase envelope. The new method indicates this type of indefinite situations, where the fluid is unstable ($D_{SP} < 0$), but has no solution of two equilibrium phases. It is important to recognize that the P_* term depends not only on the phase properties, but also on local details of the interface that may not be described rigorously by a simple capillary pressure model.

3.4. Case 4

The TPD function of Michelsen [3] gives a stationary point with a negative TPD value inside the two-phase region. In a single-phase region of pressure, temperature, and composition space, however, the TPD function exhibits either a stationary point with a positive TPD value or no stationary point except for the reference phase (i.e., the trivial solution). The thermodynamic conditions for such stationary points with positive TPD values were referred to as a "shadow-phase region" [39]. Such a shadow-phase region occurs between the two-phase region and the region of no non-trivial stationary point. Rasmussen et al. [39] proposed a method to not perform phase stability analysis outside of the shadow phase region during EOS compositional flow simulation for computational efficiency.

In the presence of capillary pressure, however, this shadow-phase region defined by the Gibbs free energy becomes irrelevant because the Gibbs free energy is defined for a given pressure and temperature. That is, it does not describe the effect of any pressure difference between phases on the shadow-phase region. This section presents for the first time that the shadow-phase region in the presence of capillary pressure is properly defined by the Helmholtz free energy and potentially useful for computationally efficient flow simulation.

The example used is based on the "SJ15" fluid (Table 2) as shown in Fig. 9. The solid line shows the phase boundary with no capillary pressure. The thin dashed line shows the outer boundary of the Gibbs shadow-phase region by Rasmussen et al. [39] (i.e., no capillary pressure is considered). The bold dashed line shows the outer boundary of the Helmholtz shadow-phase region using the new method. The difference between the two shadow-phase regions shows the substantial effect of capillary pressure. Fig. 9 shows that the Gibbs shadow-phase region is enclosed by the Helmholtz shadow-phase region for the bubble-point side and the other way around for the dew point side. However, this observation is not general as confirmed in other cases (including the next case shown below). Fig. 9 shows three selected points, A, B, and C at 366.5 K, for which phase-split calculations are performed with different capillary pressures. Fig. 10 shows the resulting oil-phase mole fractions for Points A, B, and C for different capillary pressures. The results of phase-split calculations for point A clearly show that two-phase equilibrium is possible with a capillary pressure outside the Gibbs shadow phase region, demonstrating the inapplicability of the Gibbs shadow-phase region in the presence of capillary pressure.

Fig. 11 shows another example using the mixture given in Tables 4 and 5 Fig. 11a presents the two-phase boundary with a solid line, the outer boundary of the Gibbs shadow-phase region with a thin dashed line, and the outer boundary of the Helmholtz shadow-phase region with a bold dashed line. Fig. 11b shows three selected points, D, E, and F, at 34.5 bar, for each of which phase-split calculations are performed with different capillary pressures. Fig. 12 shows the resulting gas-phase mole fractions for Points D, E, and F for different constant capillary pressures. The hollow circle for each curve corresponds to the capillary pressure beyond which no solution exists for the phase-split calculations (positive and negative flash). Point A is on the edge of the Gibbs shadow-phase

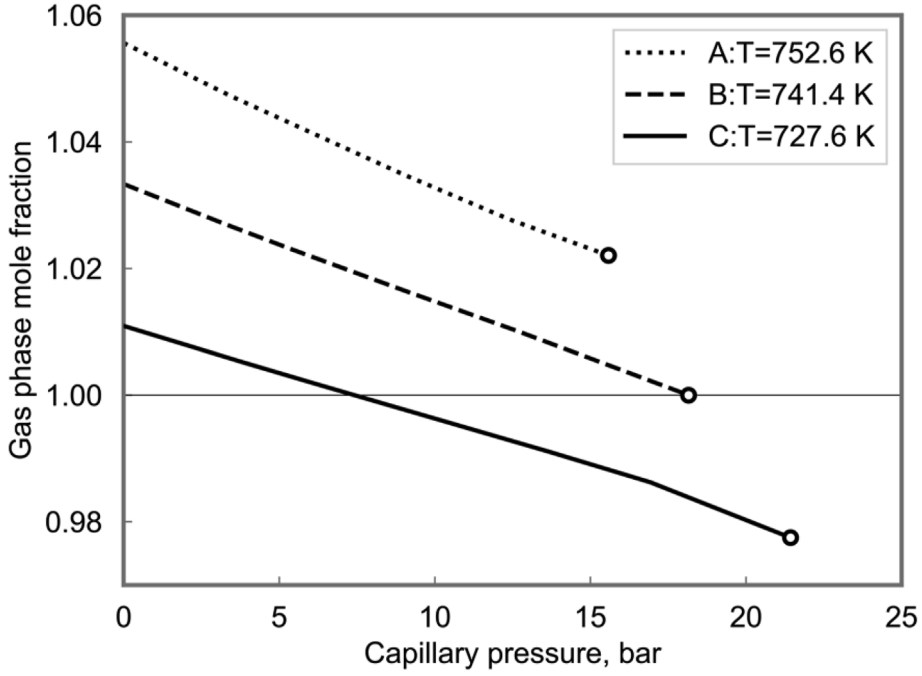

Fig. 12. Oil phase mole fractions calculated at 34.5 bar at three different temperatures, Points A, B, and C given in Fig. 11b. The temperature is 752.6 K for Point A, 741.4 K for Point B, and 727.6 K for Point C at the reference-phase pressure of 34.5 bars as indicated in Fig. 11b.

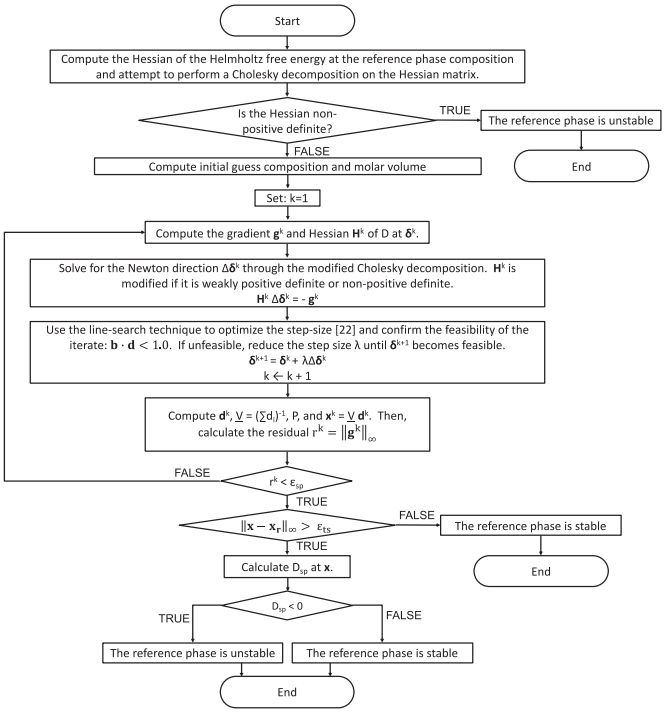

region (see Fig. 11b), but no capillary pressure value allows for a stable two-phase solution at this condition. Point B is on the edge of the Helmholtz shadow-phase region (Fig. 11b) and has a stable two-phase solution only with the capillary pressure of 34.5 bar. Point C is located deep inside the Helmholtz shadow-phase region in Fig. 11a. There is a range of capillary pressures that make stable two-phase solutions as shown by the solid line in Fig. 11b. Another example of this situation was presented previously in Fig. 4b for the simple binary system (Table 3). The D_T function shows a stationary point that is not the reference phase because it is inside the Helmholtz shadow-phase region.

4. Conclusions

This paper presented a new formulation and algorithm for phase stability analysis for tight porous media using the Helmholtz free energy. The effect of a curved interface on phase stability was rigorously considered in the formulation and algorithm developed. Case studies were presented to highlight the main differences between the new method and recently proposed methods of phase stability analysis. Conclusions are as follows:

- Results in this paper demonstrated the inherent consistency between the Gibbs-based and the Helmholtz-based formulations for phase stability analysis in the presence of capillary pressure. It is important to recognize and implement in the algorithm that the term "$-(P-P_r)+P_*$" becomes zero only if $dA_{total}=0$ for any perturbation of $\mathbf{d}$; i.e., an equilibrium state.
- The conventional methods using the Gibbs free energy cause various difficulties in phase stability analysis with capillary pressure. Application of the traditional TPD analysis using the Gibbs free energy gives a region of negative TPD values because of a non-physical part of the Gibbs free energy for the lower-pressure phase. The fundamental cause of this issue is that the Gibbs free energy in composition space requires a pressure to be specified.
- Another type of difficulty with the conventional methods is when phase-split calculations do not converge as part of the phase stability analysis with capillary pressure. Cases were presented for the overshoot of the iterative capillary pressure and non-existence of two-phase solution with a high capillary pressure.
- The new method using the Helmholtz free energy does not have the issues mentioned in items 2 and 3 above. The new method only involves one Helmholtz free energy surface in the variable space, in which the variability of pressure is inherently considered. Unlike the conventional methods, the new method requires neither the iterative capillary pressure nor phase-split calculations.
- It is shown for the first time that there exist indefinite situations in phase stability analysis with capillary pressure, in which the fluid is unstable, but has no solution of two equilibrium phases. This indefinite solution is related to the description of the P_* term as shown in Section 2.1. This P_* term depends not only on the equilibrium phase properties, but also on local details of the interface that may not be described rigorously by a simple capillary pressure model.
- It is demonstrated for the first time that the shadow-phase region in the presence of capillary pressure can be defined with the Helmholtz free energy. Case studies show that the traditional shadow-phase region based on the Gibbs free energy is invalid in the presence of capillary pressure.

Declaration of competing interest

The authors declare that they have no known competing financial interests or personal relationships that could have

appeared to influence the work reported in this paper.

CRediT authorship contribution statement

Sofiane Haythem Achour: Conceptualization, Methodology, Software, Validation, Investigation, Writing - original draft, Writing - review & editing, Visualization. **Ryosuke Okuno:** Conceptualization, Methodology, Validation, Writing - original draft, Writing - review & editing, Supervision, Project administration, Funding acquisition.

Nomenclature

Roman symbols

a_o	Saturation-based capillary pressure parameter defined in Appendix C
a_g	Saturation-based capillary pressure parameter defined in Appendix C
a	Interfacial area
A	Helmholtz free energy
b_o	Saturation-based capillary pressure parameter defined in Appendix C
b_g	Saturation-based capillary pressure parameter defined in Appendix C
b_i	Co-volume parameter for the Peng-Robinson equation of state
b	Vector containing the co-volume parameter for the Peng-Robinson equation of state
d_{ij}	Molar density for component i in phase j
d	Vector containing the component molar densities
D	Stability determinant function defined in section 2.1
D_T	Stability determinant function defined in section 3.2
f_{ij}	Fugacity of component i in phase j
F_i	ith stationarity condition for the D function defined in section section 2.1
g	Gradient of the D function
$\underline{G}_R$	Dimensionless molar Gibbs free energy
H	Hessian matrix
k	Permeability of a porous medium
N_c	Number of components
P	Pressure
P_*	Term defined in section 2.1
P_{cap}	Capillary pressure
r	Residuals used to determine convergence
R	Ideal gas constant
$\mathscr{R}$	Capillary tube radius
S_j	Volumetric saturation for phase j
T	Temperature or equation for the tangent plane to a surface
V	Volume
$\underline{V}$	Molar volume
x_{ij}	Mole fraction for component i in phase j
x	Vector containing component mole fractions in a mixture

Greek letters

γ	Parachor exponent
γ	Phase-dependent parameter in the TPD derived by Kou and Sun [23]
δ_{ij}	Independent variable for stability analysis for component i in phase j
$\boldsymbol{\delta}$	Vector containing independent variable for stability analysis for all the components
ε	Tolerance for convergence criterion
θ	Contact angle
λ	Step-size for minimization algorithm
Π_i	Parachor coefficient for component i
ρ_j	Mass density for phase j
σ	Interfacial tension or other interfacial property when used as a subscript
ϕ	Porosity of a porous medium

Superscripts

k	Index for iteration steps

Subscripts

g	Gas
L	Liquid
min	Minimum
o	Oil
r	Reference
R	Reduced
SP	Stationary point
t	Trial phase
total	Total mixture property
T	Negligible interfacial energy
w	Water

Abbreviations

BIP	Binary interaction parameters
EOS	Equation of state
IFT	Interfacial tension
PR	Peng-Robinson
PT	Pressure-temperature
TPD	Tangent-plane distance
TV	Temperature-volume

Appendix E. Supplementary data

Supplementary data to this article can be found online at https://doi.org/10.1016/j.fluid.2020.112648.

Appendices

Appendix A. Interfacial tension model

The parachor model is used to compute the liquid-vapor IFT. This model is based on the critical scaling theory and has been demonstrated to accurately model oil and gas IFT by several authors [48–50]. It can be written as

$$\sigma = \left(\sum_{i=1}^{N_c} \Pi_i (d_{iL} - d_{iV}) \right)^{\gamma}, \tag{A-1}$$

where Π_i and γ are the parachor coefficient for component i and the parachor exponent. The parachor exponent was estimated to be 3.88 by Schechter and Guo [50] with a comprehensive dataset. Schechter and Guo's value is used for most of our example cases.

Appendix B. Young-Laplace capillary pressure

The Young-Laplace capillary pressure model assumes that the rock behaves as a bundle of tubes with a chemically uniform surface and constant capillary radius $\mathscr{R}$.

$$P_{cap} = 2\sigma \cos\theta / \mathscr{R} \ , \qquad \text{(B-1)}$$

where θ is the contact angle between the rock surface and the liquid-vapor interface. It is measured through the denser phase [51]. Reservoir rocks are often liquid-wet, for which $\cos\theta$ is positive.

When the Young-Laplace model is used for phase behavior calculations for tight porous media, the porous medium is assumed to be a bundle of capillary tubes with a uniform capillary radius and wettability. This seems to be the most frequently used capillary pressure model in the literature. However, this model does not represent real rocks, which have complex heterogeneous wettability and pore structure. The value of the capillary pressure depends on the location of the interface inside the heterogeneous porous medium of interest.

Appendix C. Saturation-based capillary pressure

The Young-Laplace model does not account for a pore size distribution and wettability heterogeneity. Two solutions are available that include these important effects: pore-network simulations (PNS) and saturation-based models. In PNS methods, the structure of the porous medium is used to include the path-dependency from dynamic imbibition [33] or incipient phase appearance. However, they are not commonly used in reservoir simulators because of their computational cost.

An alternative approach to modeling capillary pressure in a real rock is to use a correlation to relate capillary pressure to the position of the interface in the porous medium through the phase-saturations. It is also possible to model path-dependency in reservoir simulation with these functions [52]. The capillary pressure can also be scaled for varying fluid and rock properties using Leverett J-type functions [53]. A saturation-based model, which takes into account all the effects mentioned above, was presented by Neshat et al. [28] as follows:

$$P_{cap}(S_o) = \sigma\sqrt{\phi/k}\left(b_o \Big/ (S_o + S_w)^{a_o} + b_g \Big/ (S_g)^{a_g}\right), \qquad \text{(C-1)}$$

where ϕ and k are respectively the porosity and the permeability of the porous medium. The parameters a_o, b_o, a_g, and b_g are fitting parameters, which allow the user to fit the model to experimentally measured capillary pressure data. The parameters S_o, S_w, S_g are the oil, water, and gas volumetric phase saturations.

One aspect of these saturation based capillary pressure models is that they increase asymptotically near residual saturations. In order to avoid calculating infinite capillary pressures, Neshat at al [11]. suggested using a maximum value corresponding to the Young-Laplace capillary pressure at the minimum measurable pore-size $\mathscr{R}_{min}$. The maximum pore size $\mathscr{R}_{max}$ can also be used to limit the minimum value of the capillary pressure. Hence the oil saturations used for capillary pressure vary from S_{omin} to $1 - S_{gmin}$, where $P_{cap}(S_{omin}) = 2/\mathscr{R}_{min}$ and $P_{cap}(S_{gmin}) = 2/\mathscr{R}_{max}$.

Appendix D. Flow chart for the phase stability analysis using the Helmholtz free energy

References

[1] U.S. Energy Information Administration, Annual Energy Outlook 2019: with Projections to 2050, 2019. https://www.eia.gov/outlooks/aeo/pdf/aeo2019.pdf.

[2] L.E. Baker, A.C. Pierce, K.D. Luks, Gibbs energy analysis of phase equilibria, SPE J. 22 (5) (1982) 731–742, https://doi.org/10.2118/9806-PA.

[3] M.L. Michelsen, The isothermal flash problem. Part I. Stability, Fluid Phase Equil. 9 (1) (1982) 1–19, https://doi.org/10.1016/0378-3812(82)85001-2.

[4] J.A. Trangenstein, Customized minimization techniques for phase equilibrium computations in reservoir simulation, Chem. Eng. Sci. 42 (12) (1987) 2847–2863, https://doi.org/10.2118/949039-G.

[5] S.M. Walas, Phase Equilibria in Chemical Engineering, Butterworth Publishers, Boston, Massachussets, 1985.

[6] D.R. Perschke, Equation of State Phase Behavior Modeling for Compositional Simulation, PhD dissertation, the University of Texas at Austin, Austin, Texas, 1988.

[7] Y.B. Chang, Development and Application of an Equation of State Compositional Simulator, PhD dissertation, the University of Texas at Austin, Austin, Texas, 1990.

[8] R. Okuno, Modeling of Multiphase Behavior for Gas Flooding Simulation, PhD dissertation, the University of Texas at Austin, Austin, Texas, 2009.

[9] D. Zhu, S. Eghbali, C. Shekhar, R. Okuno, A unified algorithm for phase-stability/split calculation for multiphase isobaric-isothermal flash, SPE J. 23 (2) (2018) 498–521, https://doi.org/10.2118/175060-PA.

[10] J.S. Rowlinson, B. Widom, Molecular Theory of Capillarity, Oxford University Press, Oxford, United Kingdom, 1982.

[11] G.D. Barbosa, M.L. D'Lima, S.M. Daghash, M. Castier, F.W. Tavares, L. Travalloni, Cubic equations of state extended to confined fluids: new mixing rules and extension to spherical pores, Chem. Eng. Sci. 184 (2018) 52–61, https://doi.org/10.1016/j.ces.2018.03.047.

[12] A.A. Shapiro, E.H. Stenby, Thermodynamics of the multicomponent vapor-liquid equilibrium under capillary pressure difference, Fluid Phase Equil. 178 (1–2) (2001) 17–32, https://doi.org/10.1016/S0378-3812(00)00403-9.

[13] M. Rezaveisi, K. Sepehrnoori, G.A. Pope, R.T. Johns, Thermodynamic analysis of phase behavior at high capillary pressure, SPE J. 23 (6) (2018) 1438–1451, https://doi.org/10.2118/175135-PA.

[14] M. Sherafati, K. Jessen, Stability analysis for multicomponent mixtures including capillary pressure, Fluid Phase Equil. 433 (2017) 56–66, https://doi.org/10.1016/j.fluid.2016.11.013.

[15] S.S. Neshat, R. Okuno, G.A. Pope, Thermodynamic stability analysis of multi-component mixtures with capillary pressure, in: Presented at the SPE Reservoir Simulation Conference, Galveston, Texas, 10-11 April, 2019, https://doi.org/10.2118/193888-MS.

[16] C.H. Whitson, M.L. Michelsen, The negative flash, Fluid Phase Equil. 53 (1989) 51–71, https://doi.org/10.1016/0378-3812(89)80072-X.

[17] N.R. Nagarajan, A.S. Cullick, A. Griewank, New strategy for phase equilibrium and critical point calculations by thermodynamic energy analysis. Part I. Stability analysis and flash, Fluid Phase Equil. 62 (3) (1991) 191–210, https://doi.org/10.1016/0378-3812(91)80010-S.

[18] M.L. Michelsen, R.A. Heidemann, Calculation of critical points from cubic two-constant equations of state, AIChE J. 27 (3) (1988) 521–523, https://doi.org/10.1002/aic.690270326.

[19] J. Mikyška, A. Firoozabadi, Investigation of mixture stability at given volume, temperature, and number of moles, Fluid Phase Equil. 321 (2012) 1–9, https://doi.org/10.1016/j.fluid.2012.01.026.

[20] M. Castier, Helmholtz function-based global phase stability test and its link to the isothermal-isochoric flash problem, Fluid Phase Equil. 379 (2014) 104–111, https://doi.org/10.1016/j.fluid.2014.07.008.

[21] D.V. Nichita, Volume-based phase stability analysis including capillary pressure, Fluid Phase Equil. 492 (2019) 145–160, https://doi.org/10.1016/j.fluid.2019.03.025.

[22] D.V. Nichita, Fast and robust phase stability testing at isothermal-isochoric conditions, Fluid Phase Equil. 447 (2017) 107–124, https://doi.org/10.1016/j.fluid.2017.05.022.

[23] J. Kou, S. Sun, A stable Algorithm for calculating phase equilibria with capillarity at specified moles, volume and temperature using a dynamic model, Fluid Phase Equil. 456 (2018) 7–24, https://doi.org/10.1016/j.fluid.2017.09.018.

[24] D.V. Nichita, Density-based phase envelope construction including capillary pressure, Fluid Phase Equil. 498 (2019) 33–44, https://doi.org/10.1016/j.fluid.2019.06.018.

[25] D.R. Sandoval, M.L. Michelsen, W. Yan, E.H. Stenby, VT-based phase envelope and flash calculations in the presence of capillary pressure, Ind. Eng. Chem. Res. 58 (13) (2019) 5291–5300, https://doi.org/10.1021/acs.iecr.8b05976.

[26] D.B. Robinson, D.Y. Peng, The Characterization of the Heptane and Heavier Fractions for GPA Peng-Robinson Programs, Gas Processors Association Research Report, Tulsa, Oklahoma, 1978.

[27] J.D. van der Waals, On the Continuity of the Gaseous and Liquid States, Dover Publications, Inc., New York, 1873. Edited and with an Introduction by Rowlinson, J.S. (1988).

[28] S.S. Neshat, R. Okuno, G.A. Pope, A rigorous solution to the problem of phase behavior in unconventional formations with high capillary pressure, SPE J. 23 (4) (2018) 1438–1451, https://doi.org/10.2118/187260-PA.

[29] K.R. Christoffersen, C.H. Whitson, Gas/oil capillary pressure of chalk at elevated pressures, SPE Form. Eval. 10 (3) (1995) 153–159, https://doi.org/10.2118/26673-PA.

[30] W.R. Purcell, Capillary pressures - their measurement using mercury and the calculation of permeability therefrom, J. Petrol. Technol. 1 (2) (1949) 39–48, https://doi.org/10.2118/949039-G.

[31] G.M. Wilson, A modified Redlich-Kwong equation of state: application to general physical data calculations, in: Presented at the 65th National AIChE

Meeting, Cleveland, Ohio, 1969.
[32] D.V. Nichita, C.A. Duran-Valencia, S. Gomez, Volume-based thermodynamic global phase stability analysis, Chem. Eng. Commun. 193 (10) (2006) 1194–1216, https://doi.org/10.1080/00986440500440165.
[33] Y. Deng, L.W. Lake, Thermodynamic study of capillary pressure curves based on free energy minimization, Geofluids 1 (3) (2001) 183–193, https://doi.org/10.1046/j.1468-8123.2001.00010.x.
[34] A. Kumar, R. Okuno, Direct perturbation of the Peng–Robinson attraction and covolume parameters for reservoir fluid characterization, Chem. Eng. Sci. 127 (4) (2015) 293–309, https://doi.org/10.1016/j.ces.2015.01.032.
[35] B. Yan, Y. Wang, J.E. Killough, A fully compositional model considering the effect of nanopores in tight oil reservoirs, J. Petrol. Sci. Eng. 152 (2017) 675–682, https://doi.org/10.1016/j.petrol.2017.01.005.
[36] A. Kumar, Characterization of Reservoir Fluids Based on Petrurbation from N-Alkanes, PhD dissertation, the University of Alberta, Edmonton, Alberta, 2016.
[37] A. Orangi, N.R. Nagarajan, M.M. Honarpour, J.J. Rosenzweig, Unconventional shale oil and gas-condensate reservoir production, impact of rock, fluid, and hydraulic fractures, in: Presented at the SPE Hydraulic Fracturing Technology Conference, the Woodlands, Texas, 24-26 January, 2011, https://doi.org/10.2118/140536-MS.
[38] C. Xu, C. Torres-Verdín, Petrophysical rock classification in the cotton valley tight-gas sandstone reservoir with a clustering pore-system orthogonality, Interpretation 2 (1) (2014) 13–23, https://doi.org/10.1190/INT-2013-0063.1.
[39] C.P. Rasmussen, K. Krejbjerg, M.L. Michelsen, K.E. Bjurstrøm, Increasing the computational speed of flash calculations with applications for compositional, transient simulations, SPE Reservoir Eval. Eng. 9 (1) (2006) 32–38, https://doi.org/10.2118/84181-PA.
[40] A.I. Brusilovsky, Mathematical simulation of phase behavior of natural multicomponent systems at high pressures with an equation of state, SPE Reservoir Eng. 7 (1) (1992) 117–122, https://doi.org/10.2118/20180-PA.
[41] B. Nojabaei, R.T. Johns, L. Chu, Effect of capillary pressure on phase behavior in tight rocks and shales, SPE Reservoir Eval. Eng. 16 (3) (2013) 281–289, https://doi.org/10.2118/159258-PA.
[42] Y. Wang, B. Yan, J. Killough, Compositional modeling of tight oil using dynamic nanopore properties, in: Presented at the SPE Annual Technical Conference and Exhibition, New Orleans, Lousisiana, 30 September-2 October, 2013, https://doi.org/10.2118/166267-MS.
[43] D.R. Sandoval, W. Yan, M.L. Michelsen, E.H. Stenby, The phase envelope of multicomponent mixtures in the presence of a capillary pressure difference, Ind. Eng. Chem. Res. 55 (22) (2016) 6530–6538, https://doi.org/10.1021/acs.iecr.6b00972.
[44] N. Siripatrachai, T. Ertekin, R.T. Johns, Compositional simulation of hydraulically fractured tight formation considering the effect of capillary pressure on phase behavior, SPE J. 22 (4) (2017) 1046–1063, https://doi.org/10.2118/179660-PA.
[45] D.R. Sandoval, W. Yan, M.L. Michelsen, E.H. Stenby, Influence of adsorption and capillary pressure on phase equilibria inside shale reservoirs, Energy Fuels 32 (3) (2018) 2819–2833, https://doi.org/10.1021/acs.energyfuels.7b03274.
[46] H. Sun, H.A. Li, A new three-phase flash algorithm considering capillary pressure in a confined space, Chem. Eng. Sci. 193 (2019) 346–363, https://doi.org/10.1016/j.ces.2018.09.013.
[47] C. Lu, Z. Jin, H.A. Li, A two-phase flash algorithm with the consideration of capillary pressure at specified mole numbers, volume and temperature, Fluid Phase Equil. 485 (2019) 67–82, https://doi.org/10.1016/j.ces.2018.09.013.
[48] C.F. Weinaug, D.L. Katz, Surface tensions of methane-propane mixtures, Ind. Eng. Chem. 35 (2) (1943) 239–246, https://doi.org/10.1021/ie50398a028.
[49] S.T. Lee, M.C.H. Chien, A new multicomponent surface tension correlation based on scaling theory, in: Presented at the SPE Enhanced Oil Recovery Symposium, Tulsa, Oklahoma, April 15-18, 1984, https://doi.org/10.2118/12643-MS.
[50] D.S. Schechter, B. Guo, Parachors based on modern physics and their uses in IFT prediction of reservoir fluids, SPE Reservoir Eval. Eng. 1 (3) (1998) 207–217, https://doi.org/10.2118/30785-PA.
[51] E.J. Peters, Advanced Petrophysics: Dispersion, Interfacial Phenomena, Greenleaf Book Group, Austin, Texas, 2012.
[52] J.E. Killough, Reservoir simulation with history-dependent saturation functions, SPE J. 16 (1) (1976) 37–48, https://doi.org/10.2118/5106-PA.
[53] M.C. Leverett, Capillary behavior in porous solids, Trans AIME 142 (1) (1941) 152–169, https://doi.org/10.2118/941152-G.